ASSEMBLY AND REUSE OF AROMATIC THERMOSETTING COPOLYESTER

Jacob Meyer, PhD
ATSP Innovations, Inc.

Abstract

ATSP Innovations, Inc., Houston, TX, has developed a new family of high performance vitrimeric resins called Aromatic ThermoSetting coPolyesters (ATSP), which have Tg's ranging from 174-310C. Vitrimers are crosslinked polymers featuring dynamic covalent chemistry which allows changes in network topology via thermally-driven bond exchange. Subsequent process operations after cure are mediated by a bond exchange reaction, which normally have a fixed topology. However, when heated above their Tg - we see a transition from viscoelastic solid to viscoelastic liquid, facilitating thermoplastic-like processing, such as compression, extrusion, and laminated molding. These vitrimeric properties also means that the thermoset can be recycled like thermoplastic resins. ATSP Innovations, Inc. has developed molding compounds, continuous fiber composites, coatings, and extremely versatile alloys, which are currently in use in the aerospace industry. The molding compounds also show a combination of processability, material properties, and tribological performance that makes them attractive for challenging friction/wear and bearing surface applications. ATSP continuous-fiber composites show outstanding creep resistance, thermal stability, and interlaminar toughness properties which make them ideal for many robust composite automotive component applications.

Background

Interchain transesterification reactions (ITR) are unique to polymers with ester linkages and have been found to aid in the formation of bonds between molecular chains [1-4]. This can be exploited to obtain adhesive bonds between polymers with ester linkages [5]. Surface reactions can occur at elevated temperatures to form chemically contiguous network chemical bonds.

Bond exchange reactions, of which ITR is a constituent member, have several distinctive features. These include that the functional groups present before and after the reaction are identical and that the reaction is reversible [6]. Bond exchange reactions (also known as chemical interchange reactions, transreactions, and dynamic covalent reactions [7]) are not unique to polyesters and are, in fact, conceptually plausible in many polymers and a number of schemes have been identified [8]. Other interchange reactions in condensation polymers so far identified include those among polyamides between amide and amine functional groups and between amide groups [7-9]. Interchange reactions have been identified among siloxanes in the presence of strong base or sulfuric acid [9-10]. Interchange reactions in polysulfides are known to occur between 1) thiol and disulfide bonds, 2) adjacent disulfides, and 3) inorganic and organic disulfides, which produces mercaptan [9,11]. These have been proposed as a stress-relief mechanism in vulcanized rubbers under strain at elevated temperatures [12]. Imine exchange [13-14], Diels-Alder reactions [15], olefin and alkyne metathesis [8,16] have also been studied. The term vitrimers was created by the Ludwik Liebler group at the Centre National de la Recherche Scientifique (CNRS) to describe thermoset polymers possessing exchangeable bonds [17]. This class of polymers features additional processability due to their ability to undergo topology changes within the covalent network. However, the first polymer system deliberately conceived of to exploit these features was developed in the James Economy group at the University of Illinois at Urbana-Champaign (UIUC) in the 1990's [5,18].

Exchange reactions within the polyester backbone can be classed into three types. The first type is an exchange reaction between a hydroxyl end group with a neighboring ester that is termed an alcoholysis reaction [6] and is completely reversible at every step. This reaction proceeds by nucleophilic addition of the hydroxyl to a carbonyl group of an ester linkage. This process induces a positive charge to the hydroxyl oxygen and a negative charge to the carbonyl oxygen. The intermediate structure expels an alcohol via electron transfer from the negatively-charged oxygen which captures a proton from the original hydroxyl. The final result is that exchange occurs at the carbon-oxygen single bond in the original ester [19]. Flory previously demonstrated that presence of an acid catalyst enabled ready reaction of copolymers in excess decamethylene glycol and adipic acid, which produced hydroxyl terminated polymers. This reaction was determined by inferring a decrease in molecular weight to the copolymer by observing a viscosity decrease with decamethylene glycol monomer addition to the high MW polymer melt. This type exchange reaction in polyesters is commercially exploited for the synthesis of polyethylene terephthalate from ethylene glycol and terephthalic acid [20].

Figure 1.1 and the lower portion of Figure 1.2 demonstrate the second type of exchange reaction observed for polyesters: acidolysis. This reaction proceeds by nucleophilic addition in a similar manner as described for alcoholysis above wherein an acyl oxygen on a carboxylic acid adds to a carbonyl of a backbone ester. Again, the tetrahedral intermediate of the original polyester acyl oxygen eliminates an ester linkage formed between the original ester oxygen and the carbonyl of the original carboxylic acid. This reaction also produces a new carboxylic acid [19]. An example of use of this class of reaction is the reaction of PET with 4-acetoxybenzoic acid (4-ABA) to produce a copolymer [21]. It was assumed in this study that only acidolysis proceeded, however that may not be a valid assumption due to the possibility that the third class of ester exchange reactions occurred between the acetoxy unit of the 4-ABA and the ester backbone units of the high MW PET.

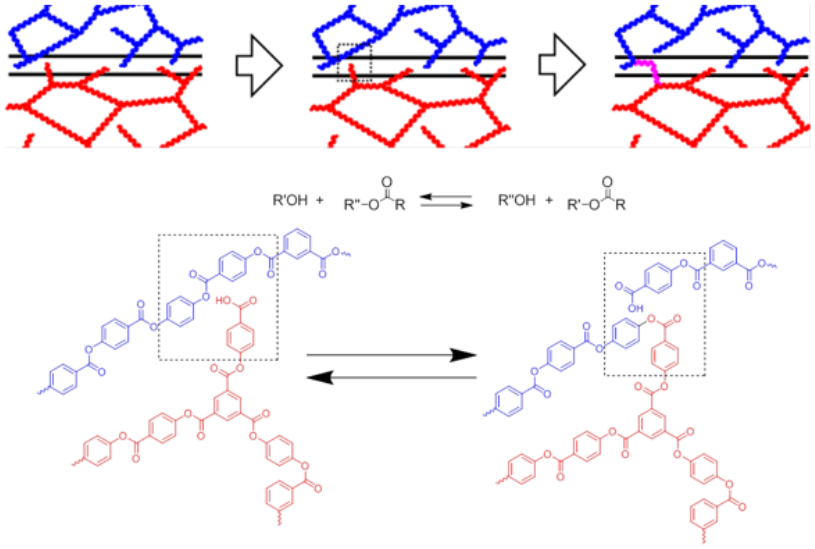

Figure 1. Example chemical reaction at surface between carboxylic acid and ester unit via acidolysis. An example reaction for surface-surface bonding of crosslinked aromatic polyesters.

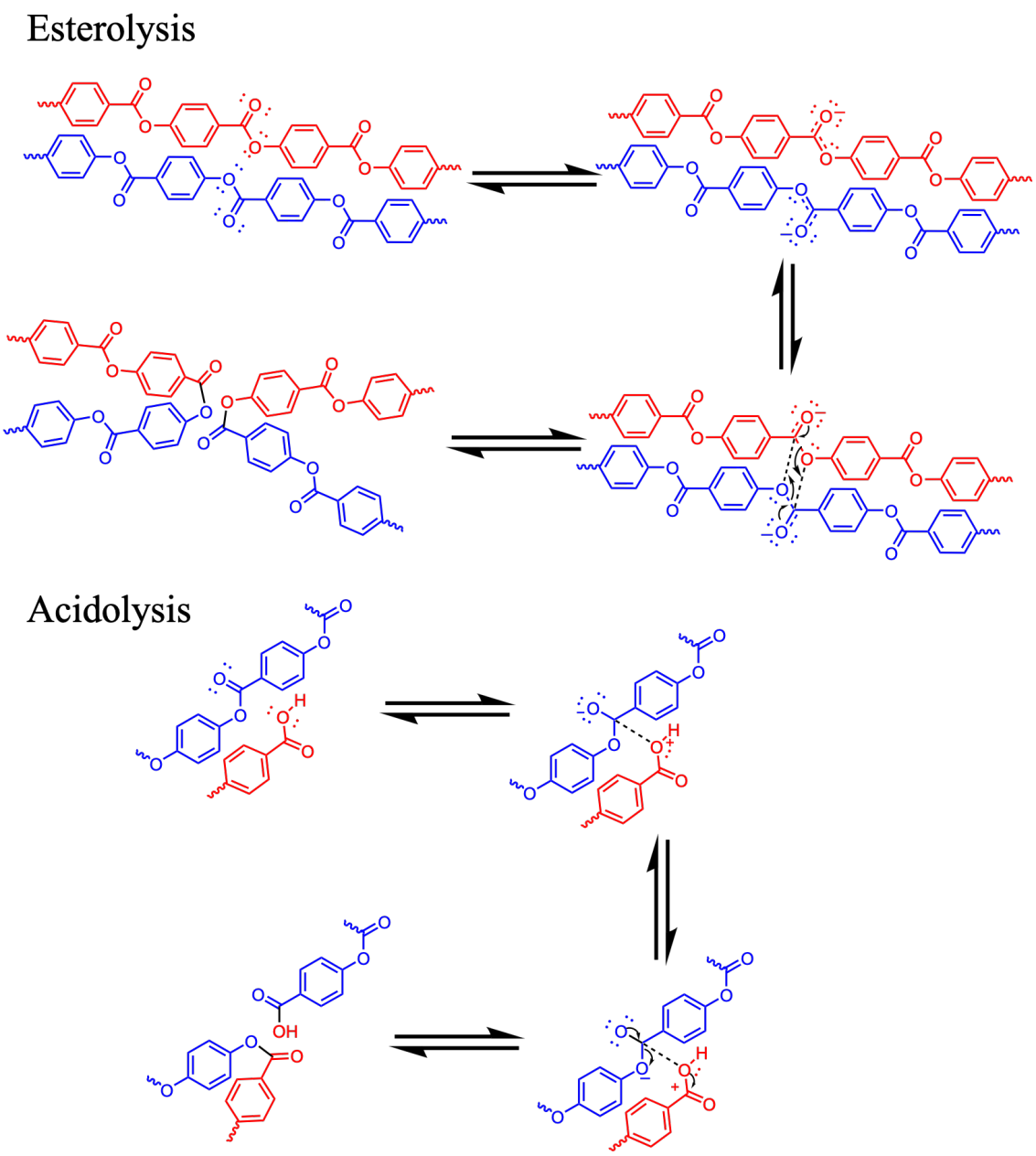

Figure 2. Proposed interchain transesesterification reaction mechanisms in aromatic polyesters for esterolysis and acidolysis.

Ester-ester exchange, known as esterolysis, is the third mechanism for ITR in polyesters. An example reaction for aromatic polyesters is shown in the upper portion of Figure 1.2. Rather than the nucleophilic pathways for alcoholysis and acidolysis, this exchange reaction is thought to proceed by what is termed an associative reaction mechanism [22-23]. Two carbonyls of adjacent ester bonds experience formation of an association complex and the acyl groups of the original esters are switched. While Flory and others [9,24-25] have suggested that evidence indicates that esterolysis proceeds very slowly, contradictory evidence exists [23,26,27] for exchange of PET and bisphenol-A diacetates. These were determined both through NMR and viscosity changes.

All-aromatic thermosetting copolyesters are prepared using a set of carboxylic acid-capped and acetoxy-capped crosslinkable aromatic copolyester oligomers [18,53]. These two oligomer groups (noted in literature as C-type for carboxylic acidcapped and A-type for acetoxy capped) are synthesized using different molar ratios of hydroquinone diacetate (HQDA), resorcinol diacetate (RDA), biphenol diacetate (BPDA), p-acetoxybenzoic acid (ABA), isophthalic acid (IPA), and trimesic acid (TMA) as key building blocks. The heat-induced condensation polymerization reaction is enabled through mixing the two oligomer sets at particular weight ratios in solid-state and carrying out a rationally designed thermal cure process. The polycondensation reaction generates the crosslinked aromatic polyester backbone of the matrix while releasing acetic acid as a reaction by-product. The proposed reaction mechanism is shown in Figure 1.7 below. The crosslinked aromatic polyesters can be produced in either amorphous or liquid crystalline formulations by selection of appropriate monomer feed ratio to select crosslink density [37].

ATSPs are a high temperature resin that has unique properties [1-5,7,9]. Prior experiments demonstrate ATSP has better thermal stability and low moisture pickup compared to epoxies, with properties equivalent to those of best performing thermoset polyimides [12-15] and can be repaired more easily than either [21]. ATSP is stable in air at 350 C and in nitrogen at 425 C [4,20] whereas most thermally stable epoxies decompose at 170-190 C in air or nitrogen. The moisture pickup of the resin is relatively low (0.3 wt%, as compared to 2.3% for epoxy and 2.6% for polyimides) [12-15], increasing the potential durability against physical ageing. ATSP also shows outstanding flame [42] and ablative character [9] which may be of utility in the design of high performance structures.

Experimental

Coated and carbon fiber composite specimens were produced using the four different ATSP formulations. For the coated specimens, uncured matching oligomers of ATSP were coated on aerospace grade Al 7075 parts (Figure 2.3) using an electrostatic powder coating technique. The samples were subjected to thermal curing followed by thickness measurement of the unbonded ATSP-coated adherends by an eddy-current-based coating thickness gauge. For the carbon fiber composites, the laminae were produced using a VARTM method previously described in [3], where they were cured in a vacuum bag in a convection oven with a peak temperature of 330°C. A unidirectional fabric of Sikawrap 103C by Hexcel was used as the carbon fiber preform.

Thermal Stability

Thermal stability of representative clippings of ATSP composite specimens will be measured in a TA Instruments TGA 2950 ramped at 10 °C/min to 600 °C in air, N2, and CO2 to replicate a wide range of potential mission atmosphere conditions. The trace of the mass loss/temperature derivative curve as well as the total mass loss will be reported. Additional high temperature hold experiments at 371 °C for one hour in air will be conducted with mass loss as a percentage reported as point of comparison with VARTM polyimide composites from Cano et al. [7].

Temperature Dependent Strength and Modulus

Mechanical strength and modulus of the composites will be determined by short beam shear strength (SBS) following ASTM D2344, and flexural strength and modulus following ASTM D790. An Instron mechanical testing machine with temperature shroud will be used with a test speed of 1.27 mm/min. Flexural tests will carried out at a test speed of 0.76 mm/min using the same load cell and temperature shroud. Temperature points of -90 °C, RT, and 180 °C will be used for this matrix of experiments for comparison with state of art composite materials and published literature [5-8].

Temperature Dependent Fracture Toughness

Fracture toughness will be determined by double cantilever beam (DCB) configuration specimens with a pre-crack introduced during the cure process by thin polyimide film to conform to ASTM D5528. An Instron machine operating in displacement-controlled mode with a crosshead displacement speed of 0.67 mm/s will be used with an end-tab configuration affixed by solid state bonded ATSP applied to the end tab to provide a high temperature adhesive [19]. Composite specimens will be 20 to 25 mm wide and at least 125 mm long and 3 mm thick. Temperature points of -90 °C, RT, and 100 °C will be used for the matrix of experiments.

Results and Discussion

Dynamic mechanical analysis (DMA) was performed in a TA Instruments DMA Q800 to obtain the storage modulus and Tg of ATSP via a 3 °C/min temperature ramp with a 1 Hz oscillation. Neat ATSP specimens were cut to 25 mm long by 7 mm wide by 1 mm thick and were loaded in a tensile clamp configuration. Dynamic thermal mechanical data as the storage modulus, loss modulus and tan δ as a function of temperature are shown in Figure 12. The glass-transition temperature (Tg) reported based on the tan δ peak was about 239.3 °C for C1A1 and 253.5 °C for C2A2, and 307 °C for CBAB. As expected, the Tg of the material decreased with an increase in molecular weight. As molecular weight increases, the resultant crosslink density decreases which will result in a lowering of the Tg.

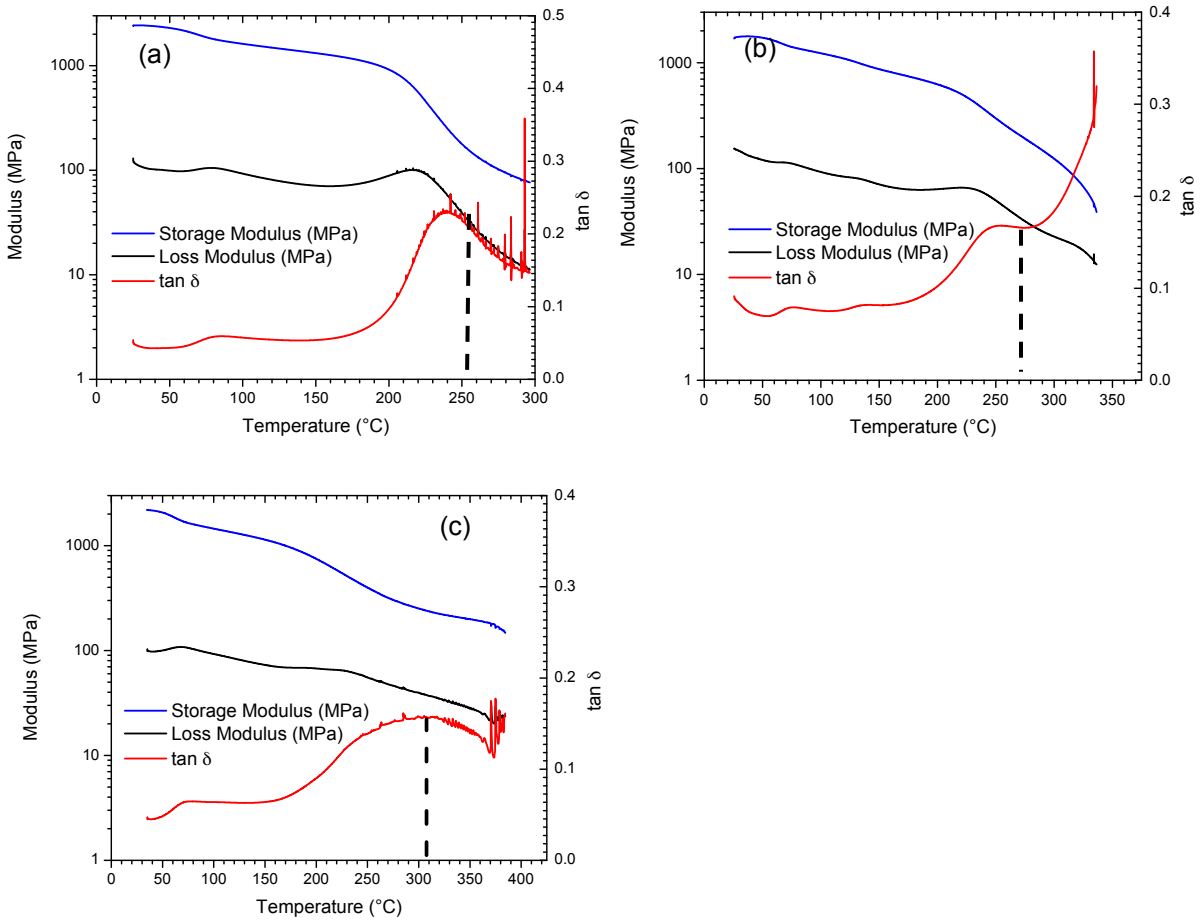

Figure 12. DMA results for neat ATSP samples, (a) C1A1, (b) C2A2, and (c) CBAB.

Cryogenic dynamic thermal mechanical data as the tan δ as a function of temperature for C1A1 and C2A2 neat polymers at different frequencies are shown in Figure 13. The tan δ peak at

around 0 and -50 °C was observed for C1A1 and C2A2, respectively.

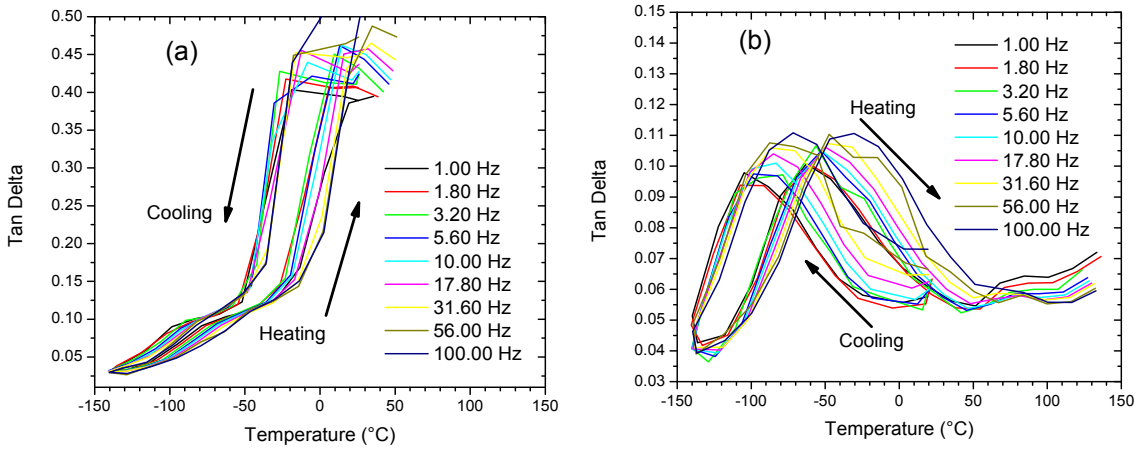

Figure 13. Cryogenic DMA results for neat ATSP samples, (a) C1A1, (b) C2A2.

Thermogravimetic analysis (conducted on a TA Instruments TGA 2950) was also used to study the thermal stability of the C1A1/C, C2A2/C and CBAB/C composites. ATSP composites were cut and tested in the TGA under nitrogen and air at heating rates of 10 °C/min. Figure 14 shows the trace of the mass loss/temperature derivative curve as well as the total mass loss. The composites were stable even above 400 °C which reiterates the high temperature stability of this resin system. The weight loss was about 60, 67 and 62% for C1A1/C, C2A2/C and CBAB/C composites at 800 °C, respectively in air and about 27% for all composites in nitrogen.

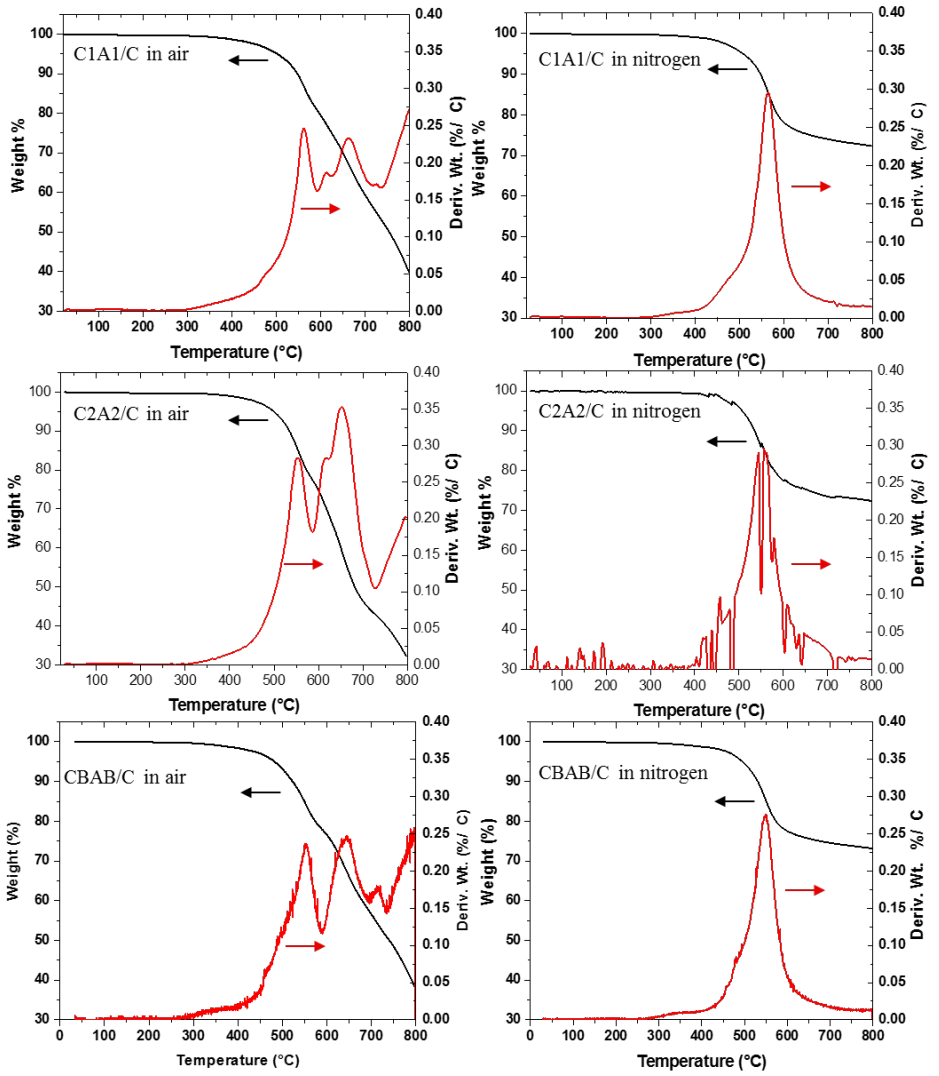

Figure 14. TGA curves of C1A1/C, C2A2/C and CBAB/C composites in air and nitrogen.

Isothermal heat stability of ATSP at 371 °C was also characterized for C1A1/C, C2A2/C and CBAB/C composite. The ATSP/C samples were ramped up to 371 °C at a rate of 10 °C/min and then held isothermally at that temperature for 1 hour in an air atmosphere. The weight loss at this temperature was about 3.52, 3.05, and 1.33% for C1A1/C, C2A2/C and CBAB/C composites, respectively (Figure 15). Note that in the temperature range of testing, carbon fiber is stable and should not contribute to the weight loss. Some high temperature polyimides mass loss are presented in Table 5. As shown, CBAB/C lost just 1.33% of its weight was. Even though C1A1 and C2A2/C mass loss at 371 °C was about 1 % higher than that of polyimides (Table 5) [7], one should note that the polyimides were cured at 371 °C for one hour during processing while ATSP final cure temperature was at 330 °C.

Table 5. Cured Tg after 1 hour at 371°C and mass loss.

Material	Tg (°C)	Mass Loss (%)
PETI-8/1000	301	2.78
PETI-8/1125	293	2.24
PETI-8/1250	275	1.42
C1A1/C	239	3.25
C2A2/C	253	3.05
CBAB/C	307	1.33

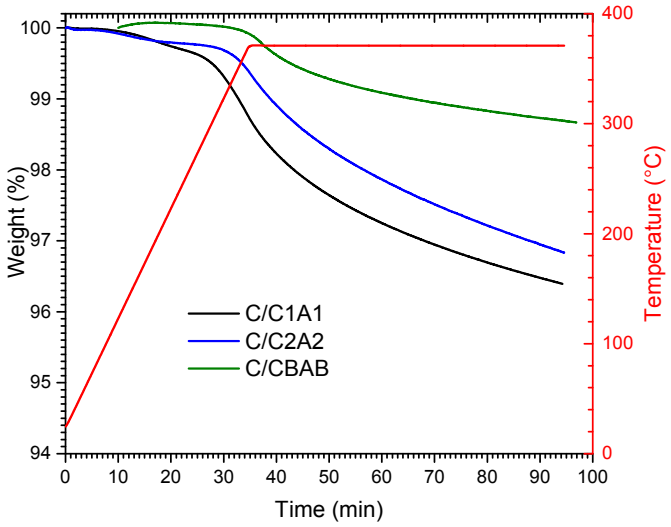

Figure 15. Isothermal heat stability of ATSP/C composites.

Coefficient of Thermal Expansion

CTEs for composite specimens was measured on a Dilatometer. ATSP (C1A1/C and C2A2/C) and 8551-7/C samples were sectioned into 3 x 3 x 25 mm blocks. The specimen was placed in a dilatometer between a quartz fixture with a constant normal force that held onto the sample. The temperature was increased at a rate of 5°C/min from RT to 300 °C. Change in displacement with increasing temperature curves for ATSP and reference samples are shown in Figure 16. CTE for both longitudinal and transverse sections of ATSP composites as well as [0/90]2s layup of ATSP and 8551-7/C are reported in Table 6.

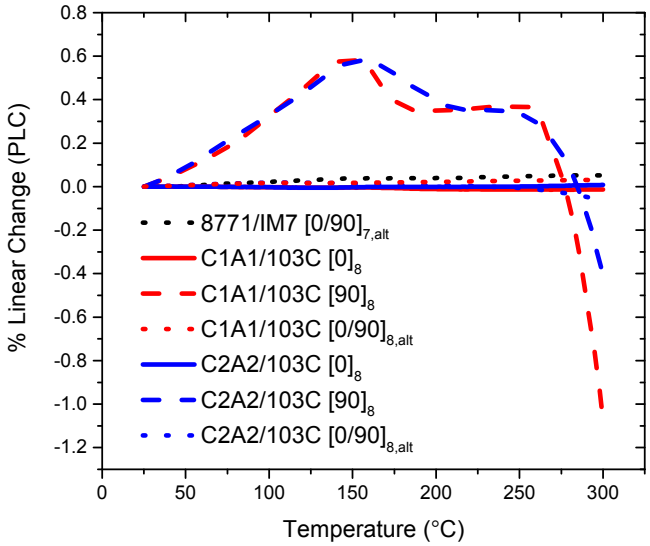

Figure 16. Change in displacement with increasing temperature plot for ATSP and reference composites.

Table 6. CTE of ATSP and 8551-7/C composites.

Composite	Fiber Volume (%)	Longitudinal CTE (1/K)	Transverse CTE (1/K)	[0/90]s CTE (1/K)
C1A1/C	63.7	-4.73 x 10-7	46 x 10-6	1.17 x 10-6
C2A2/C	56.7	2.98 x 10-7	50 x 10-6	1.4 x 10-6
8551-7/C	60	-	-	1.91 x 10-6

The CTE of 8551-7/C is higher than that of ATSP/C composites. We expect that the residual stresses induced in ATSP/C composites will be lower than that of 8551-7/C, thus ATSP/C can help in providing reliable composite structures when used over a range of temperatures.

Flexural Stress and Modulus

Four point flexural tests of the ATSP composites were conducted according to ASTM D7264 at room temperature with the loading rate of 2 mm/min, as shown in Figure 17. This procedure involved arranging cured lamina in unidirectional configurations [0°] which were then solid-state bonded using ITR at a temperature of 330 °C for 4 h under a compressive pressure of 100 psi under vacuum. Finished laminates were then cut into specimens of 130 mm in length for testing. The width and thickness of samples are shown in Table 7. Flat rectangular specimens, 8-ply unidirectional fabrics, of (C1A1/C and C2A2/C) composites were loaded in 4-point bending Instron machine.

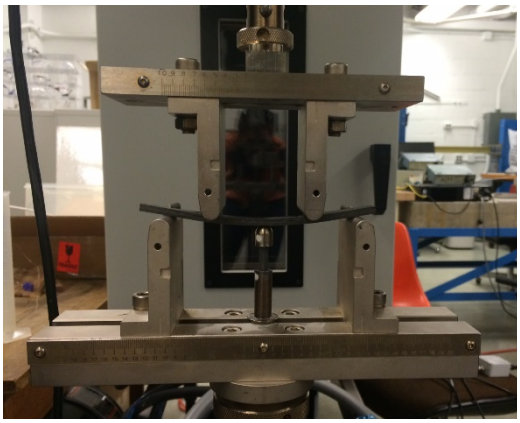

Figure 17. Flexural testing being conducted.

Flexural strength, σ, and modulus, Ef, of the composites were calculated using the following equations: (4) $$\sigma = \frac{3PL}{4bh^2}$$

where, P is the breaking force of the specimen, L is the span support (105 mm), b is the width and h is the thickness.

The flexural modulus, Ef, is calculated by drawing a tangent to the steepest initial straight-line portion of the load deflection curve and using the following equation:

(5) $$E_f = \frac{0.17L^3m}{bh^3}$$

where m is the slope of tangent of the initial straight-line portion of the load deflection curve.

A minimum of five tests were conducted for each chemistry, and the average values and variations are presented in Table 7. The stress–strain curve from sample # 1 is also shown in Figure 18. Note that the load increases linearly until the failure point.

Table 7. Flexural properties of C1A1/C and C2A2/C composites.

Sample ID#	Resin Chemistry	Flexural Stress (MPa)	Flexural Modulus (GPa)	b (mm)	h (mm)	span/thickness L/h
1	C1A1	993.7	120.5	13.03	4.00	26.25
2	C1A1	1161.0	114.1	12.10	3.97	26.45
3	C1A1	1262.0	127.7	12.88	3.88	27.06
4	C1A1	877.9	108.7	12.76	3.80	27.63
5	C1A1	1111.1	125.2	12.50	3.90	26.92
Mean	**C1A1**	**1081.1**	**119.2**	**12.7**	**3.9**	**26.9**
Standard deviation	**C1A1**	**149.1**	**7.8**	**0.4**	**0.1**	**0.5**
7	C2A2	879.0	119.4	12.22	2.25	46.67
8	C2A2	712.9	108.1	13.22	2.97	35.35
9	C2A2	660.9	109.8	13.80	2.82	37.23
10	C2A2	759.5	108.3	13.10	2.20	47.73
11	C2A2	770.9	115.4	12.25	2.23	47.09
12	C2A2	841.1	109.2	14.11	2.34	44.87
Mean	**C2A2**	**770.7**	**111.7**	**13.1**	**2.5**	**43.2**
Standard deviation	**C2A2**	**80.3**	**4.6**	**0.8**	**0.3**	**5.4**

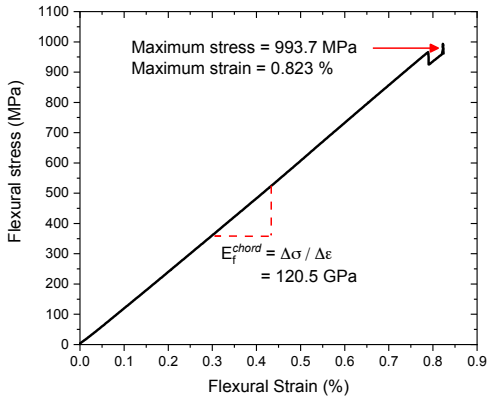

Figure 18. Stress-strain curve from flexural test (sample #1).

Following the testing, all specimens were inspected. As shown in Figure 19, the most common failure in nearly all composites was compressive local buckling at the outer (top) surface between the loading noses. The C1A1/C composites evidenced a flexural strength and moduli of 1081.1±149.1 MPa and 119.2±7.8 GPa, respectively which is comparable or better than that of polyimide and epoxy/carbon unidirectional composites available in literature [7, 23-24]. Therefore, we can gain the qualitative observation that out-of-plane shear moduli and strength should be fairly high. This becomes an effective demonstration of the ability of fully-cured ATSP laminae to be bonded together via interchain transesterification reactions (ITR) into an effective multi-ply laminate.

C2A2 composites evidenced a somewhat lower flexural strength than C1A1-based composites for one of two reasons: produced C2A2 composites were generally thinner in the thickness dimension that C1A1 composites while the test was still conducted with a specified span length, resulting in a change in span ratio (span length versus thickness, Table 7). This may have created an earlier onset of failure events due to an increase in compressive stress concentration at the upper surface (inside curvature) due to overall great deflection of the C2A2 samples during testing.

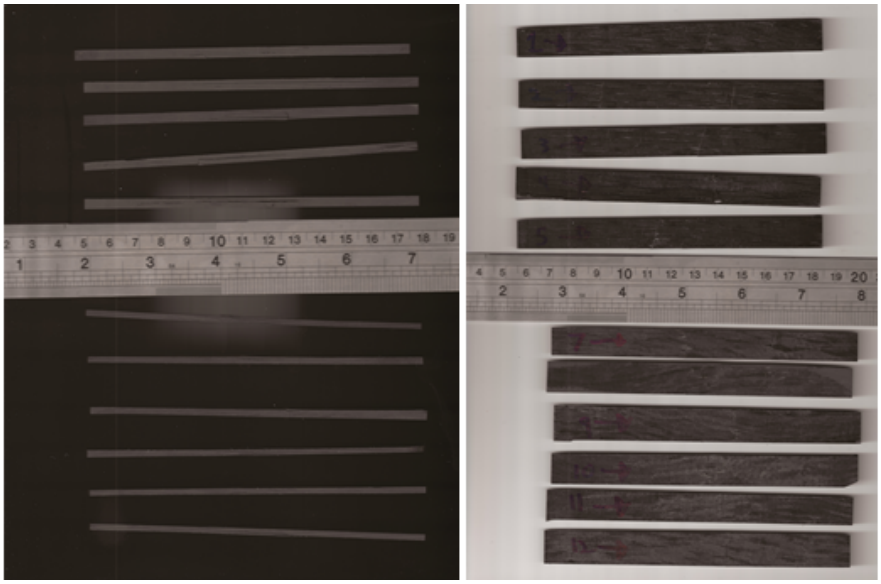

Figure 19. C1A1 (top) and C2A2 (bottom) specimens after flexural tests.

Temperature Dependent Fracture Toughness

The fracture toughness and damage resistance of ATSP composites was characterized as shown in Figure 20. Composite specimens, 20 mm wide, 3 mm thick and at least 125 mm long, with [0/90/0]s layup pattern was used for testing ATSP matrices. A precrack was introduced in the sample during the ITR cycle by placing a PTFE ply between the lamina. The samples were loaded under tension and the two faces were pulled apart at a constant rate of 2 mm/min. The fracture toughness of C1A1/C and C2A2/C was determined by loading a double cantilever beam sample under tension at -90, RT and 100 °C. Samples were allowed to equilibrate with their environment for 5 minutes prior to testing. A representative curve of the load vs displacement is shown in Figure 21. For each sample the load was calculated as the average of the loads for up to 90 mm of delamination length.

The GIc values of the various samples were calculated. The results are summarized in Table 8, and a representative Mode I fracture toughness versus delamination length curve for C2A2/C composite is shown in Figure 22.

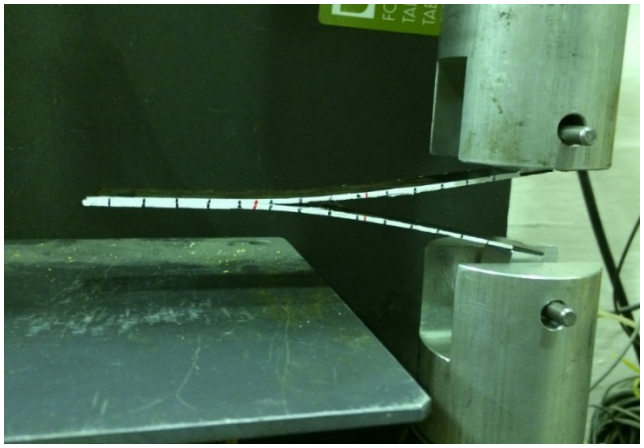

Figure 20. Fracture toughness testing being conducted.

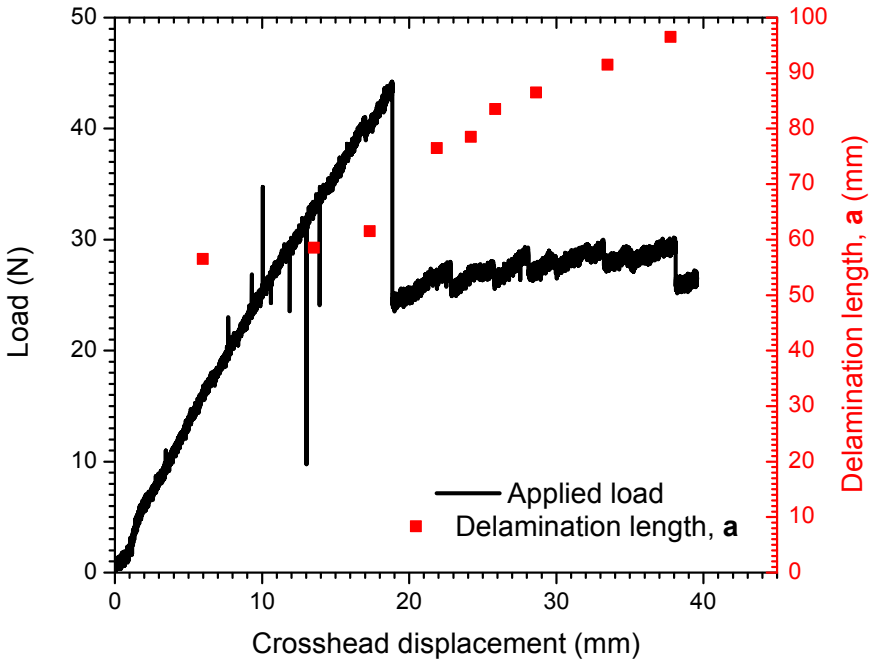

Figure 21. Representative load vs displacement and delamination length vs displacement curves for C2A2/C composite obtained during fracture toughness testing a 100 °C.

Table 8: Interlaminar fracture toughness properties of ATSP/C composites

Composite	Layup	Temperature °C	G I c K J / m 2 (Mean)
C1A1/C	[0/90/0]s	RT	320.0
C2A2/C	[0/90/0]s	RT	429.8
C1A1/C	[0/90/0]s	100 ± 5	653.0
C2A2/C	[0/90/0]s	100 ± 5	749.6
C1A1/C	[0/90/0]s	-90 ± 5	332.5
C2A2/C	[0/90/0]s	-90 ± 5	457.7

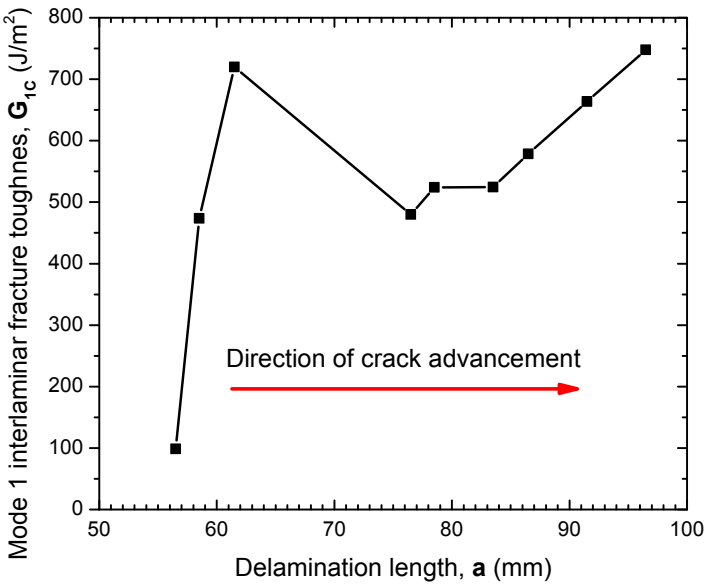

Figure 22. Representative Mode I fracture toughness vs delamination length curve for C2A2/C composite at 100 °C.

Calculated GIc values were obtained via modified beam theory (MBT) as given in section 13.1.1 in ASTM D5528 with modifications for compliance and loading block geometry recommended in Annex A1. Results indicate that both C1A1 and C2A2-based composites based on laminae joined via solid-state ITR reactions evidenced fracture toughness values comparable or better than existing epoxy composites. This demonstrates the viability of solid-state bonding via the ITR mechanism for fabrication of composite structures. Both C1A1 and C2A2, as well, evidenced no significant decline at cryogenic and elevated temperatures, indicating the potential for their use within elevated temperature and cryogenic conditions. There was a modest enhancement of properties observed for C2A2 (which was based on liquid crystalline oligomers and which continues to evidence birefringence in the fully cured state) versus amorphous C1A1. This is thought to have physical origin in one or both of (1) elevated void content for C1A1 composites, or (2) local microfibrillation and enhanced cusping in C2A2 as suggested by the persistence of markers of liquid crystallinity from the oligomeric to the fully cured state and ex situ observations of fracture surfaces of C2A2 relative to C1A1.

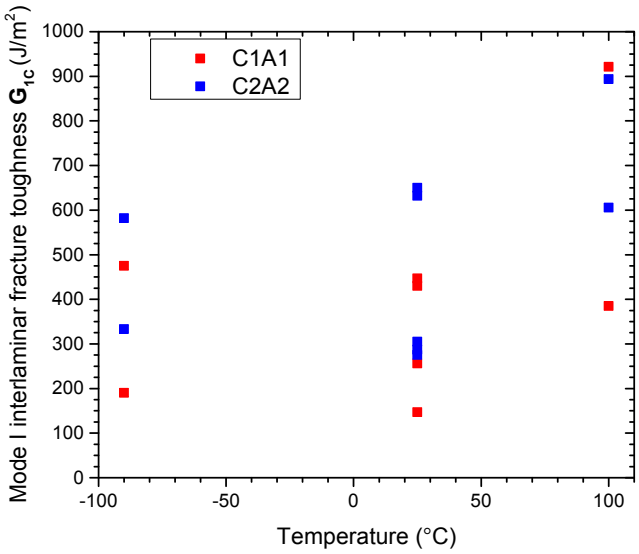

Figure 23. Temperature dependence of Mode I interlaminar fracture toughness of ATSP/C composites

Summary and Next Steps

Research was conducted to demonstrate novel approaches, technical feasibility, and performance characterization for low-cost, durable aromatic thermosetting copolyester (ATSP) composites. Based on the advancements that have been achieved, our efforts going forward will focus on accelerating the transition of this technology out of the lab and into industry with emphasis on demonstrable manufacturing that can be scaled up for very large structures. The overall objective of this project is to develop a superior performance material for future commercial applications utilizing the unique ATSP resin system.

Bibliography

1. Lopez and J. Economy, *Polym. Compos.*, **2001**, 22, 444.
2. D. Frich, A. Hall, J. Economy, *Macromol. Chem. Phys.*, **1998**, 199, 913.
3. J. Economy, L. A. Schneggenburger, *Macromolecular Symposia*, **1998**, 128, 1.
4. L. A. Schneggenburger, P. Osenar, and J. Economy, *Macromolecules*, **1997**, 30, 3754.
5. D. Frich, J. Economy, K. Goranov, *Poly Eng. and Sci*, **1997**, 37, 541.
6. T. Davies, “Chemical Reactions of Polymers”, *Interscience*, **1964**, 553.
7. F. Calleja, S. Fakirov, H. Zachmannm, Ed: S. Fakirov, “Transreactions in Condensation Polymers”, *Wiley-VCH*, **2008**, 429-473.
8. Y. Jin, C. Yu, R.J. Denman, W. Zhang, *Chem. Soc. Rev.*, **2013**, 42, 6634.
9. P. Flory, “Principles of Polymer Chemistry”, *Cornell University Press*, 1953.

10. M. Berenbaum, “Chemical Reactions of Polymers”, *Interscience*, **1964**, 528.
11. E. Bostick, “Chemical Reactions of Polymers”, *Interscience*, **1964**, 515.
12. M. Stern and A. Tobolosky, *J. Chem. Phys.,* **1946**, 14, 93.
13. P. Taynton, C. Zhu, S. Loob, R. Shoemaker, J. Pritchard, Y. Jin, W. Zhang, *Polym. Chem*., **2016**,7, 7052.
14. A. Chao, I. Negulescu, D. Zhang*, Macromolecules,* **2016**, 49, 17, 6277.
15. R.C. Boutelle, B.H. Northrop, *J. Org. Chem*., **2011**, 76, 19, 7994.
16. G.C. Vougioukalakis, R.H. Grubbs, *Chem. Rev*., **2010**, 110, 3, 1746.
17. M. Capelot, M.M. Unterlass, F. Tournihac, L. Liebler, *ACS Macro Lett*., **2012**, 1, 7, 789.
18. D. Frich, K. Goranov, L. Schneggenburger, J. Economy, *Macromolecules,* **1996**, 29, 24, 7734
19. J. McMurry, “Organic Chemistry”, 8th Ed., *Brooks Cole*, **2011**.
20. M. Stevens, “Polymer Chemistry: An Introduction”, 3rd Edition, *Oxford University Press*, **1999**.